Mechanism of the Unfolding of Transmembrane α-Helical Segment (1−36)-Bacteriorhodopsin Studied by Molecular Dynamics Simulations

Dmitry M. Korzhnev, Vladislav Yu. Orekhov, and Alexander S. Arseniev*

Shemyakin and Ovchinnikov Institute of Bioorganic Chemistry, Russian Academy of Sciences, Ul. Miklukho-Maklaya 16/10, Moscow, 117871, Russia

Rainer Gratias and Horst Kessler

Institute of Organic Chemistry and Biochemistry, Technical University Munich, Lichtenbergstr. 4, D-85747 Garching, Germany

Received: January 22, 1999; In Final Form: May 11, 1999

The unfolding of the first transmembrane segment 1−36 bacteriorhodopsin (BR) was studied using 1.25 ns molecular dynamics (MD) simulation with an explicit representation of chloroform/methanol 1:1 mixture and a series of long (from 10 to 60 ns) Langevin dynamics (LD) simulations. Comparison of MD and LD simulations shows that the random and frictional forces of Langevin equation provides a good model for the weakly polar chloroform/methanol mixture. The dielectric permeability $\epsilon_o = 1-2$ ($\epsilon = \epsilon_o r$) was found to be suitable for the modeling of the shielding effect of a weakly polar solvent in the LD simulations. The enhancement of short-range electrostatic interactions stabilizes the α-helix in LD simulations. The α-helix unfolding proceeds through the formation of local regions, stabilized by π-helical hydrogen bonds (π-bulges), in the central part of (1−36)-BR. Being formed, the π-bulges can propagate to metastable structures with partially solvated backbone intermediates on the way to an α-helix−random coil transition. Two regions of the π-bulges formation within (1−36)-BR are attached to the Leu-Gly-Thr sequence.

Introduction

Folding of membrane proteins is proposed to be a two-stage process.[1] The first stage is the independent formation of stable α-helices, penetrating the membrane bilayer; the second is their association into a tightly packed complex. The transmembrane α-helices are suggested to behave as autonomous folding domains. This suggestion is confirmed by numerous experiments on membrane proteins refolding[2−4] and NMR studies of isolated transmembrane α-helices in membrane-mimicking media (as a review see Pervushin and Arseniev[5]). The further understanding of the mechanisms of the membrane proteins folding requires data on the formation of isolated transmembrane α-helices and the specificity of helix−helix recognition.

The molecular dynamics simulations are widely used for studying the formation and unfolding of α-helices. The numerous simulations of α-helical homopolymers and isolated α-helices of globular proteins were performed in water. The simulations show that the formation of the α-helices proceeds through a number of intermediate stages. Tobias and Brooks[6] have shown that reverse turns serve as intermediates in the formation of the first helix turn within the coil region. The study of the pathways of α-helix growth shows that N-terminal growth is more preferable and proceeds through 3_{10}-helix.[7] Intermediates with 3_{10}-helical hydrogen bonds and different water-mediated structures were observed in molecular dynamics simulations of the unfolding of α-helices in water.[8−13] In water isolated α-helices of globular proteins are usually unstable without tertiary interactions.[14] In some cases simulations are performed in water/thrifluoroethanol mixtures to get more stable molecular dynamics trajectories.[11,15] However, as a rule, the helices partially or completely unfold within nanoseconds independently of the solvent composition.

Although recently there has been considerable progress in molecular dynamics simulations of transmembrane α-helices with an explicit representation of the medium,[16−22] the formation of α-helices in membranes and organic solvents mimicking the membrane media is not as well studied as in water. The mechanisms of the unfolding of α-helices of membrane proteins differ from those reported for water-soluble peptides. Kovacs et al.[16] observed the unfolding through the π-helix, starting from the C-terminal part of the α-helix. The formation of π-helical regions within the transmembrane α-helix was reported by Duneau et al.[22,23]

The nonpolar low-dielectric membrane environment promotes the helical conformation and ensures the high stability of the transmembrane segments of integral membrane proteins.[24,25] The structures of transmembrane segments are rich in the strong helix breakers Gly and Pro. These residues and β-branched Ile, Val, and Thr modulate the helicity of the segments in the membrane medium and are thought to be responsible for the conformation transitions during the functioning of the membrane protein.[24,26,27] Thus, the knowledge of the mechanisms of the formation and unfolding of transmembrane segments could also clarify some aspects of membrane protein functions.

In this paper we study mechanisms of unfolding of the first transmembrane segment 1−36 bacteriorhodopsin (BR) using molecular dynamics simulation with an explicit representation of a chloroform/methanol mixture and several Langevin (stochastic) dynamics simulations. The segment (1−36)-BR can be regarded as the minimal autonomous folding subunit of bacte-

* To whom correspondence should be addressed: Phone: +7(095) 330-5929. Fax: +7(095) 335-5033. E-mail: aars@nmr.ru.

10.1021/jp990262r CCC: $18.00
Published on Web 07/30/1999

riorhodopsin. Indeed, in the lipid bilayer BR can be reformed from the peptides containing this segment, the second helix, and the complementary five-helical fragment.[3] In a recent molecular dynamics study Gratias and Kessler[28] developed a chloroform/methanol system suitable for simulations of transmembrane peptides in the membrane-mimicking environment. The simulation of (1−36)-BR in this system allows for the direct comparison of the observed results with the available experimental data on the segment structure and dynamics.[29−31] In this work special attention is focused on the factors affecting the peptide stability, the solvent effect on the helix dynamics, and the molecular mechanism of the α-helix unfolding.

Methods

Molecular Dynamics Simulation. Molecular dynamics (MD) simulation of (1−36)-BR (pQAQITGR**PEW IWLALGTALM GLGTLYFLVK GM**GVSD; residues of transmembrane part Pro8−Met32 are bold) in a 1:1 chloroform/methanol mixture, with explicit account of the solvent, was performed with the MSI program suite Discover and the CVFF force field.[32] The flexible three-site potential model of methanol and the four-site model of chloroform molecules were used for the representation of the solvent.[28] The NMR structure of (1−36)-BR[29] was placed in a preequilibrated $45 \times 75 \times 45$ Å^3 periodic box with 475 chloroform and 693 methanol molecules. The details of the box generation and equilibration were described by Gratias and Kessler.[28] All hydrogen atoms of the peptide were explicitly included in the calculations. The ionization states of charged residues were set to mimic a neutral pH environment (Asp, Glu were ionized; Lys, Arg were protonated). The simulation was carried out with a 1 fs time-step. The nonbonded interactions were smoothly turned off in the interval between 12.5 and 13.5 Å. Constant dielectric permeability of $\epsilon = 1.0$ was used for modeling the electrostatic interactions. The simulation includes two parts. In the first part, a preliminary *NPT* simulation with the peptide atoms fixed at their positions was performed to reach the optimal solvation of the structure. After several cycles of energy minimization and heating of the system to 303 K by increasing the temperature every 1 ps by 50 K, the system with the molecule fixed was equilibrated for 100 ps. Direct velocity scaling algorithm for temperature adjustment and coupling to a 1.0 bar pressure bath[33] with a relaxation time of $\tau_p = 0.1$ ps and isothermal compressibility of $\beta = 5.0 \times 10^{-5}$ bar^{-1} were applied during this part of the simulation. Then several cycles of minimization of the equilibrated system with the fixed molecule were carried out followed by 4000 steps of steepest descent minimization with the unconstrained peptide. In the second part an *NVT* simulation with the unconstrained peptide was performed. After heating the system to 303 K the simulation of 1.25 ns length was carried out using a weak coupling to the heat bath with a time constant of 0.1 ps. The coordinates for analysis were saved every 1.0 ps.

Langevin (Stochastic) Dynamics Simulations. A series of long Langevin dynamics (LD) simulations of the first transmembrane fragment of BR were performed using the CHARMM program[34] with the version 19 parameter set. The NMR structure of (1−36)-BR[29] was taken as a starting point of the simulation. The unstructured N- and C-terminal parts (residues 1−7 and 33−36) of (1−36)-BR were excluded from the consideration. To avoid the effects of artificial terminal charges, the terminal residues Pro8 and Met32 were modified by uncharged acetamide and methylamide groups, respectively. All polar hydrogens were explicitly taken into account; the aliphatic hydrogens were treated using a united atom representation. The lengths of the bonds with hydrogen atoms were kept constant by applying the SHAKE algorithm.[35] The simulations were carried out using a 1 fs time step. Nonbonded interactions were smoothly turned off in the interval between 12 and 14 Å. Distance-dependent dielectric permeability ($\epsilon = \epsilon_o r_{ji}$) was used to model the electrostatics interactions. Five LD simulations with different dielectric permeabilities ϵ_o and temperatures have been studied: $\epsilon_o = 1$, $T = 300$ K (60 ns); $\epsilon_o = 1$, $T = 500$ K (10 ns); $\epsilon_o = 2$, $T = 300$ K (11 ns); $\epsilon_o = 4$, $T = 300$ K (11 ns); $\epsilon_o = 5$, $T = 300$ K (5 ns). In all simulations the initial velocities for atoms of the energy-minimized structure were assigned from a Maxwell−Boltzmann distribution at 5 K. The structure was heated by gradual increase of the temperature every 50 fs by 5 K. During the LD simulations the friction constants of 20 ps^{-1}, appropriate for modeling of chloroform solution,[36,37] were applied to all solute (united) atoms. The coordinates for the analysis were saved every 0.5 ps.

Results and Discussion

The combination of LD and MD simulations provides the possibility for comprehensive analysis of the events occurring during the α-helix unfolding and factors affecting the stability of the α-helix. The Langevin (stochastic) simulations significantly reduce the computational time and allow us to generate trajectories more then 1 order of magnitude longer than the solvated MD trajectory and, therefore, are suitable for statistically meaningful sampling of the motions occurring on a pico- to nanosecond time scale (see, for example, Bremi et al.[38]). The fact that chloroform/methanol mixtures are weakly polar allows us to include the influence of the solvent in the frictional and random forces of the Langevin equation of motion, and therefore, it is not necessary to treat the solvent molecules explicitly. The comparison of the behavior of the helix during the MD and LD simulations allows us to select the parameters for Langevin dynamics, appropriate for modeling of the weakly polar environment. The variation of the dielectric permeability constant ϵ_o in LD simulations allows us to address the role of short-range electrostatic interactions in the stabilization of transmembrane α-helix.

Below, after the overall analysis of MD and LD trajectories, the α-helix unfolding is discussed in terms of intramolecular hydrogen bonding. In the following sections the factors affecting the stability of the α-helix and the molecular mechanism of its unfolding are discussed. Finally, the results of the simulations are compared with the results of ^{1}H−^{15}N NMR relaxation study of the backbone dynamics of (1−36)-BR.[31]

Root-Mean-Square Deviations from the Starting Structure. The primary information on the α-helix unfolding can be obtained from overall characteristics of trajectories such as root-mean-square deviations (rmsd) from the starting structure. Figure 1 shows the rmsd from the starting structure during the simulations, calculated for backbone heavy atoms of the α-helical part of the peptide (residues 8−32). The mean rmsd value of 1.5−2.0 Å (Figure 1a) shows that the α-helical structure was conserved during the first 0.7 ns of the MD simulation. After 0.7 ns the rmsd progressively increases, indicating on the unfolding of the α-helix, and reaches 3.5 Å at 1.25 ns. The stability of the α-helix in the LD simulations strongly depends on the used dielectric permeability constant ϵ_o ($\epsilon = \epsilon_o r$) (Figure 1b). During 60 ns of LD simulation with $\epsilon_o = 1$ and $T = 300$ K the structure was remarkably stable; the rmsd was fluctuating around 1.5−2.0 Å (data not shown). During the 10 ns simulation with $\epsilon_o = 1$ and elevated temperature ($T = 500$ K) the α-helical structure was also conserved (data not shown). With the decrease

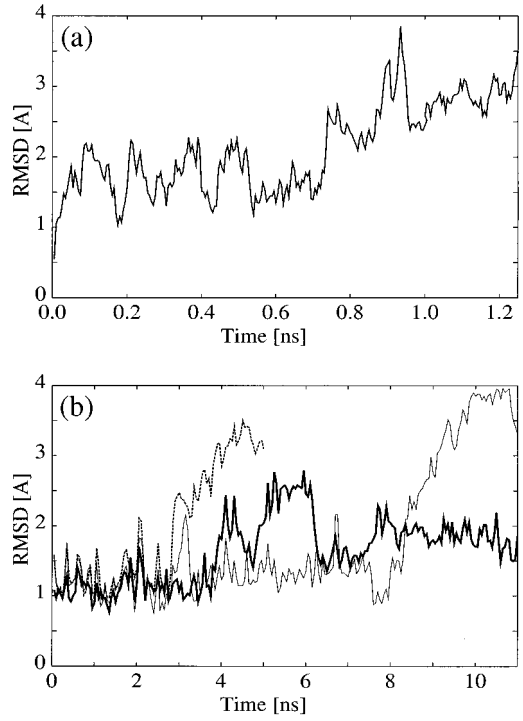

Figure 1. Root-mean-square deviations from the starting structure, calculated for backbone heavy atoms of the α-helical part (residues 8−32) of (1−36)-BR, in (a) MD and (b) LD simulations: $\epsilon_o = 2$, $T = 300$ K (bold solid line); $\epsilon_o = 4$, $T = 300$ K (thin solid line); $\epsilon_o = 5$, $T = 500$ K (dashed line).

of the electrostatic interactions the helix becomes less stable. In the LD simulation with $\epsilon_o = 2$ and $T = 300$ K the partial unfolding of the α-helix with an increase of the rmsd value to ∼2.5−3.0 Å was detected after 3.8 ns of the LD run (Figure 1b). However, the unfolding was not completed, and after 6−8 ns of the LD simulation rmsd returns to ∼2.0 Å. In the simulations with $\epsilon_o = 4$, $T = 300$ K; and $\epsilon_o = 5$, $T = 300$ K the complete loss of the α-helical structure with an increase of rmsd to 3.5−4.0 Å was detected after 8.0 and 2.5 ns, respectively (Figure 1b).

Intramolecular Hydrogen Bonds. The pathways of the α-helix unfolding are obvious after the detailed analysis of the hydrogen bond network. Figure 2 shows the populations of α-(CO_i−HN_{i+4}) and π-helical (CO_i−HN_{i+5}) hydrogen bonds during the course of selected simulations. The populations of 3_{10}-helical (CO_i−HN_{i+3}) hydrogen bonds were also analyzed (data not shown). The hydrogen bond between the potential donor and acceptor groups was considered to exist if the hydrogen−acceptor distance was less then 2.5 Å and the donor−hydrogen−acceptor angle was larger than 135°.

The analysis of the stable (according to rmsd values) parts of MD (Figure 2a) and LD (parts b−d of Figure 2) trajectories shows that α-helical hydrogen bonds, with populations of 0.6−0.9, exist in the region Pro8−Met32 of the peptide. Several $i \rightarrow i + 4$ hydrogen bonds near the N- and C-termini of the α-helix have lower populations (∼0.3−0.5). The populations of Met20−Thr24 and Leu13−Thr17 α-helical hydrogen bonds are lowered because of the formation of CO_i−$H^{\gamma 1}O_{i+4}$ hydrogen bonds between the threonine side chains in the g^+ rotameric state ($\chi^1 \approx -60°$) and carbonyl groups of Met20 and Leu13, observed by NMR techniques.[29,39] In the stable parts of all trajectories a very low (∼0.1) content of 3_{10}-helical hydrogen bonds, slightly increasing toward the N- and C-termini, was observed in the region 8−32 of the peptide. Bifurcated $(i \rightarrow i + 4)$−$(i \rightarrow i + 3)$ hydrogen bonds in the terminal parts of the α-helices and unfolding by "α-helix → 3_{10}-helix → no hydrogen bonds" mechanism were reported in numerous MD studies of isolated helical peptides in water.[8−13] However, in the case of (1−36)-BR only several terminal residues of the α-helix are involved in this reversible process.

The most interesting events of the simulations occur in the central part of the helix. After 0.7 ns of the solvated MD run two α-helical hydrogen bonds (Leu19-Gly23 and Ala18-Leu22) disappear almost simultaneously and build a π-helical hydrogen bond between CO Ala18 and NH Gly23 (Figure 2a). The π-helical region (π-bulge) progressively grows toward the N-terminus and after 0.9 ns includes three to five $i \rightarrow i + 5$ hydrogen bonds. The bifurcated $(i \rightarrow i + 4)$−$(i \rightarrow i + 5)$ hydrogen bonds on the borders of the π-bulge provide a possibility for its further growth or diminishing as well as for its shift within the α-helix. In the last part of the MD simulation (0.7−1.25 ns) fluctuations of the size and position of π-bulge were observed. In this period the boundaries of the π-helical region were defined by NH groups of Gly23−Gly24 and Ala18−Met20 residues, respectively. The formed $i \rightarrow i + 5$ hydrogen bonds have relatively high populations, reaching values of 0.5−0.7. However, their bifurcating behavior makes the π-helix region unstable. After 0.8 ns several regions, free of intramolecular hydrogen bonds, were detected near the π-bulge. It is notable that an enhanced deuterium exchange of backbone amide groups of Gly21−Thr24 residues, which are involved in π-helical hydrogen bonds after 0.7 ns of the MD simulation, was detected for (1−36)-BR in a chloroform/methanol mixture.[29]

In LD simulations the α-helix → π-helix transition strongly depends on the dielectric permeability constant ϵ_o ($\epsilon = \epsilon_o r$). During 60 ns of LD run with $\epsilon_o = 1$ and $T = 300$ K only one π-type hydrogen bond (CO Ala18−NH Gly23) was detected in several snapshots (data not shown). The formation of π-helical regions within the α-helix were observed in LD's with $\epsilon_o = 1$, $T = 500$ K; $\epsilon_o = 2$, $T = 300$ K; and $\epsilon_o = 4$, $T = 300$ K. At $\epsilon_o = 1$ and 500 K two short reversible transition to the π-helix were detected (Figure 2b). The first transition occurs during 0.35 ns after 4.2 ns of simulation; two α-helical hydrogen bonds Trp12−Gly16 and Ile11−Leu15 were replaced by the first $i \rightarrow i + 5$ bond of the π-bulge (CO Ile11−NH Gly16). The formed π-bulge was extended between NH groups of Gly16-Thr17 and Leu13-Ala14 and includes three to four π-helical hydrogen bonds. The second transition occurs during ∼0.1 ns after 4.6 ns of simulation. The mechanism of this transition is exactly the same as observed in MD simulation with explicit representation of the solvent; the first $i \rightarrow i + 5$ CO Ala18−NH Gly23 hydrogen bond was formed, and the π-bulge was extended between NH Gly23 and NH's Leu19−Met20. The mechanism of the π-bulge formation in the LD simulations with $\epsilon_o = 2$ (Figure 2c) and $\epsilon_o = 4$ (data not shown) is similar to that described above; always the first $i \rightarrow i + 5$ hydrogen bond was formed by CO Ala18−NH Gly23 or CO Ile11−NH Gly16. In the LD with $\epsilon_o = 2$ and $T = 300$ K the first CO Ala18−NH Gly23 hydrogen bond was formed after 3.8 ns of simulation (Figure 2c). The π-bulge was significantly fluctuating in size (from 3 to 8−10 $i \rightarrow i + 5$ hydrogen bonds) and moving toward the C-terminal part of the helix. After 7−8 ns of simulation the central part of (8−32)-BR returns to the α-helical structure. During the first 8 ns of LD with $\epsilon_o = 4$ and $T = 300$ K, formation of short-living π-bulges, starting from Ile11−Gly16 (four times) as well as from Ala18−Gly23 hydrogen bond (five times), was observed (data not shown). The last α-helix →

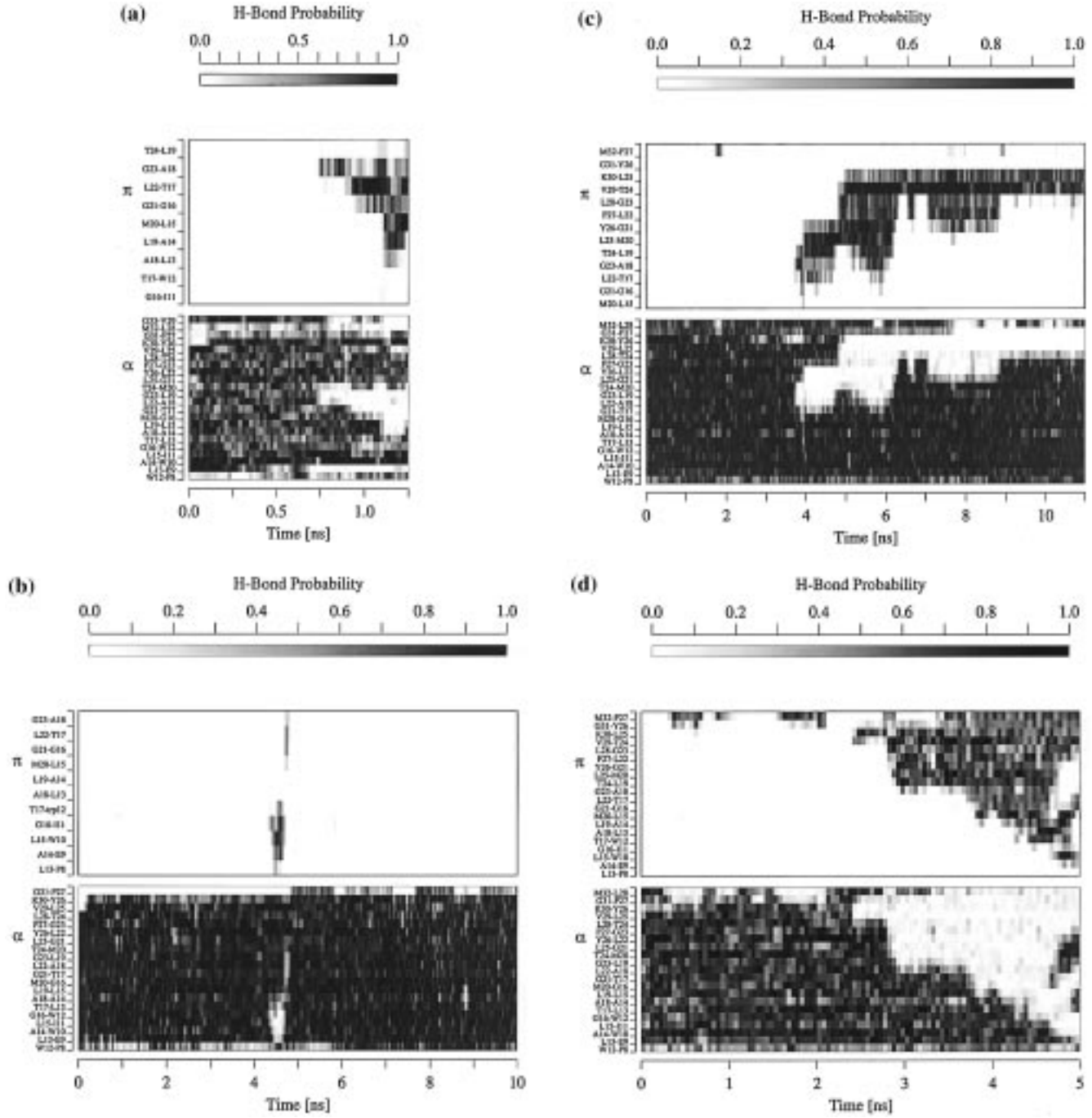

Figure 2. Populations of the backbone α-helical (CO_i-HN_{i+4}) and π-helical (CO_i-HN_{i+5}) hydrogen bonds during the course of simulations calculated for every 20 ps interval of the solvated MD trajectory and for 50 ps intervals of the LD trajectories: (a) MD; (b) LD, $\epsilon_o = 1$, $T = 500$ K; (c) LD, $\epsilon_o = 2$, $T = 300$ K; (d) LD, $\epsilon_o = 5$, $T = 300$ K.

π-helix transition, starting from the Ala18−Gly23 hydrogen bond at 8.1 ns of LD run, leads to the total disappearance of the α-helical hydrogen bond network of (8−32)-BR. The notable feature of the simulations with $\epsilon_o = 2$ and $\epsilon_o = 4$ is that during several short periods the bifurcated ($i \rightarrow i + 4$)−($i \rightarrow i + 5$) hydrogen bonds appear near the C-terminal part of the helix.

The mechanism of the α-helix unfolding in the LD simulation with $\epsilon_o = 5$ differs from the observed in LD with $\epsilon_o = 1-4$ (Figure 2d). The progressive α-helix → π-helix transition starts from the C-terminal part of the α-helix after 2.5 ns and leads to the complete loss of the α-helical structure of (8−32)-BR. The same mechanism of the α-helix unfolding was described by Kovacs et al.[16] in the MD study of surfactant protein C.

The comparison of the MD and LD simulations shows that LD with $\epsilon_o = 1-2$ ($\epsilon = \epsilon_o r$) and solvated MD provide the same mechanisms for the (1−36)-BR unfolding. Thus, the dielectric permeability $\epsilon_o = 1-2$ ($\epsilon = \epsilon_o r$) is found to be suitable for the modeling of weakly polar chloroform/methanol mixtures in Langevin dynamics simulations.

It is notable that both regions of the π-bulge formation in (1−36)-BR are attached to the Leu-Gly-Thr sequence. Namely, in the Leu_{i-1}-Gly_i-Thr_{i+1} ($i = 16, 23$) sequence the α-helical $i - 5 \rightarrow i - 1$ and $i - 4 \rightarrow i$ hydrogen bonds are replaced by the first π-helical $i - 5 \rightarrow i$ hydrogen bond. The formation of similar π-bulges was observed by Duneau et al.[23] in the MD simulations of the transmembrane domain of human c-*erb*B2 protein, pertaining to the tyrosine kinase receptor family. In the case of

c-*erb*B2 the position of the first π-helical hydrogen bond was attached to the Leu-Gly-Val sequence. The formation of a small π-bulge, termed as α-aneurism, was experimentally observed by Keefe et al.[40] during the insertion of a single glycine residue in the middle of the α-helix of staphylococcal nuclease. In the α-aneurism the amide groups of three residues, immediately following the inserted glycine residue, are involved in $i \rightarrow i + 5$ hydrogen bonds. However, the distortion of the α-helix is localized between the C^{α} atoms of the inserted glycine and the following residue. The rest of the helix practically coincides for the wild type and mutant species. Such small π-bulges provide the possibility of dynamical deletion of a single amino acid from the α-helix accompanied by turning of the π-bulge connected parts of the helix with respect to each other and shortening of the helix. In the case of (1−36)-BR short-lived (0.1−0.3 ns) small π-bulges with three to four π-helical hydrogen bonds appear several times during LD with $\epsilon_o = 1$, $T = 500$ K; and $\epsilon_o = 4$, $T = 300$ K. If the size of the π-bulge exceeds three to four $i \rightarrow i + 5$ hydrogen bonds, long-living propagated distortions of the α-helix are formed. However, the helical structure of the peptide was apparently conserved as during the formation of propagated distortions as in the case of small π-bulges. In particular no flips of backbone torsion angles were observed in the transmembrane part of (1−36)-BR in MD and LD simulations (with the exception of several very short flips of the peptide groups near Gly residues).

Stability of the π-Helix. Solvent Role in the α-Helix Unfolding. There are some reasons that make the formation of the π-helix unfavorable and that explain the rare occurrence of this motif in the protein structures. The first reason is the formation of the internal cavity in the middle of the π-helix. This is an unfavorable effect when taking into account that for a closely packed structure the gain in energy is estimated as 20 cal mol^{-1} $Å^{-2}$ of the cavity internal surface area.[41] The second reason is the slightly unfavorable backbone torsion angles $\varphi = -57°$, $\psi = -70°$ (see Kovacs et al.[16] and references therein). In addition, packing of the side chains can also account for the difference in the stabilities of π- and α-helices, where the favorable effect of the packing of C^{β} is estimated as 0.5 kcal mol^{-1} per residue.[42] On the other hand, small π-bulges, such as α-aneurism, being stabilized by $i \rightarrow i + 5$ hydrogen bonds and tertiary structure interactions, retain the structural properties of the α-helix with only minor local deviations.[40] The α-aneurism cavity has an internal surface area of <10 $Å^2$ and, therefore, practically has no effect on the stability of the structure.

For the (1−36)-BR we found a chance to form small short-lived π-bulges (three to four π-helical hydrogen bonds). In the case of the whole protein the propagation of such π-bulges can be limited by tertiary interactions. However, one can suggest that in the case of isolated helices the propagation of small π-bulges leads to metastable structures, intermediates of the α-helix to random coil transition. To test this suggestion, we compared the behavior of the propagated π-bulge with the behavior of the unstructured parts of the (1−36)-BR (residues 1−7 and 33−36) during the MD with explicit representation of the solvent. In particular, the radial distribution functions (RDF's) of different groups of the solvent molecules around the backbone NH and CO groups of the helical (8−32) and unstructured (1−7, 33−36) parts of (1−36)-BR were calculated for the stable (0.25−0.5 ns) and disturbed (0.85−1.1 ns) periods of the simulation. The RDF's of methanol OH hydrogens around the backbone oxygens of the residues from the unstructured part (Gln3 and Arg7) have sharp maxima at 1.8 Å in both considered periods (parts a and b of Figure 3). The observed peak in RDF's

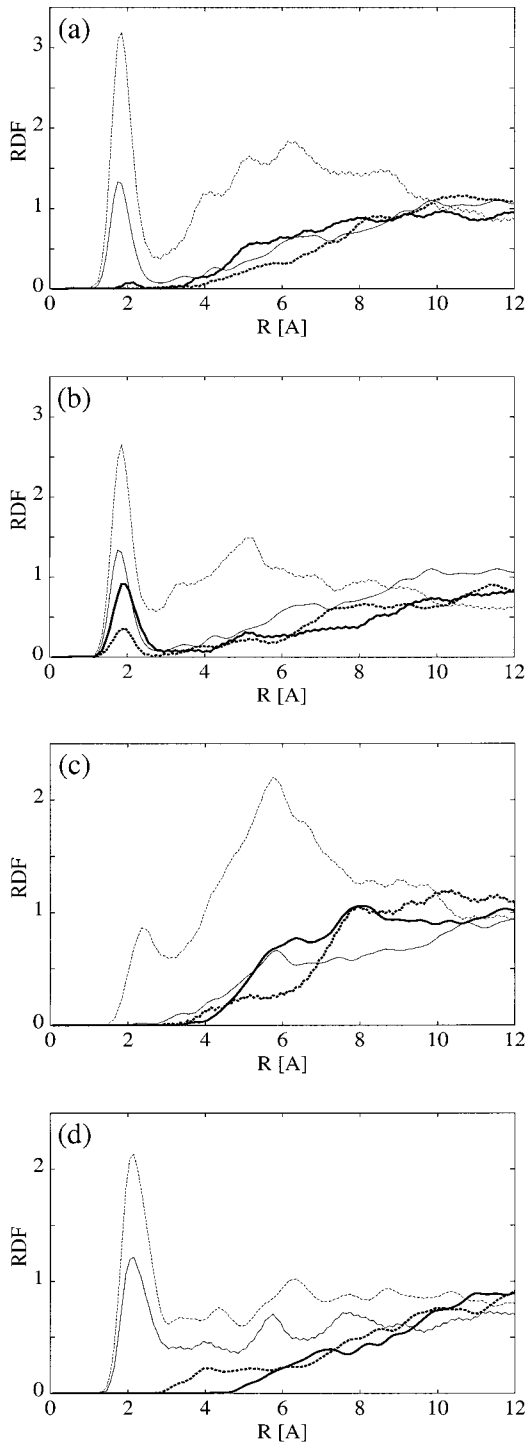

Figure 3. Radial distribution functions (RDF) of different groups of the solvent molecules around the polar groups of the (1−36)-BR backbone calculated for stable (0.25−0.5 ns) and disturbed (0.85−1.1 ns) parts of the MD trajectory: (a) 0.25−0.5 ns and (b) 0.85−1.1 ns for hydrogens of methanol OH groups around the backbone carbonyl oxygens; (c) 0.25−0.5 ns and (d) 0.85−1.1 ns for methanol oxygens around the backbone amide protons. RDF's for CO and NH groups of Gln3 and Arg7 are represented by thin solid lines and dashed lines, respectively. RDF's for CO groups of Ala18 and Leu19 are represented by bold solid lines and dashed lines, respectively. RDF's for NH groups of Leu22 and Gly23 are represented by bold solid lines and dashed lines, respectively.

suggests that CO groups of these residues participate in hydrogen bonds with methanol. Being involved in $i \rightarrow i + 4$ α-helical hydrogen bonds in the period between 0.25 and 0.5 ns, CO groups of the residues Ala18 and Leu19 are unreachable by

the solvent molecules (Figure 3a). In the period between 0.85 and 1.1 ns CO groups of Ala18 and Leu19 define the ranges of the propagated π-bulge and participate in bifurcated $i \rightarrow i + 5$ hydrogen bonds (see above). In this period the RDF's of the methanol OH hydrogens around the oxygens of Ala18 and Leu19 have a maximum at 1.8−1.9 Å, similar to that observed for carbonyl oxygens of unstructured Gln3 and Arg7 residues (Figure 3b), corresponding to hydrogen bonding with the solvent. Thus, CO groups of the residues from the propagated π-bulge are partially solvated by methanol molecules. In contrast, the RDF's of methanol oxygens around the backbone NH groups of Leu22 and Gly23, participating in π-helical hydrogen bonds in the last part of the simulation, reveal no peak corresponding to hydrogen bonding with methanol molecules (parts c and d of Figure 3). The analysis of the RDF's for Gln3 and Arg7 NH's shows that the sharp maximum at ∼2.0 Å appears only in the last part of the simulation (Figure 3d). This observation points to the fact that a proper solvation of the backbone amides in the coil state requires much more time than the solvation of carbonyls. The comparison of RDF's of chloroform chlorines around the backbone NH groups from the unstructured parts of (1−36)-BR and propagated π-bulge (data not shown) with analogous RDF's of methanol OH hydrogens (parts a and b of Figure 3) shows that the backbone NH's are preferably solvated by methanol molecules. This observation is in line with the conclusions of Gratias and Kessler[28] about the preferential solvation of polar groups in chloroform/methanol mixtures. The preferential solvation of the polar groups by an active component of the multicomponent solvent is inherent for the coil state of the polypeptide chain and plays an important role in helix−coil transition.[43,44]

The comparison of the MD and LD simulations shows that the random forces, modeling the random collisions of protein atoms with the solvent molecules, and the frictional term in the Langevin equation provide quite a good model for the weakly polar environment. The similar mechanisms of the α-helix unfolding in the MD and LD ($\epsilon_o = 1-2$) simulations suggest that the formation of the π-bulges is not caused by the specific interactions of the polar groups of (1−36)-BR with the solvent.

Mechanism of the α-Helix Unfolding. Factors Affecting the α-Helix Stability. To study the roles of residues from the Leu_{i-1}-Gly_i-Thr_{i+1} (i = 16, 23) sequence in the formation of the α-helix distortions, an analysis of events leading to the helix unfolding in MD and LD simulations was performed. An inspection of the MD and LD trajectories shows that always the same events occur during the formation of the first $i \rightarrow i + 5$ hydrogen bond of the π-bulges. Figures 4 and 5 show the events leading to the replacing of two α-helical hydrogen bonds Leu19−Gly23 and Ala18−Leu22 by the first π-helical Ala18−Gly23 hydrogen bond in the solvated MD simulation. First, at 0.65 ns a flip of the χ^1 angle of Leu22 from the t (180°) to the g^+ (−60°) rotamer occurred (Figures 4c and 5a,b). After the flip, $C^{\gamma}H$ and $C^{\delta}H_3$ of Leu22 come to close the Ala18 oxygen (Figure 4d). This event immediately leads to a slight increase of the hydrogen−acceptor distance of the Ala18−Leu22 hydrogen bond and the gradual decrease of the CO Ala18−NH Gly23 distance (Figure 4a). However, the π-bulge was only formed at 0.72 ns after the formation of the CO Met20−$H^{\gamma 1}$O Thr24 hydrogen bond competing with the backbone α-helical hydrogen bond (Figures 4e,f and 5c). After this event, changes of the hydrogen−acceptor distances and donor−hydrogen−acceptor angles indicate the replacement of the $i \rightarrow i + 4$ hydrogen bond by the $i \rightarrow i + 5$ hydrogen bond (Figures 4a,b and 5d,e). After the formation of the π-helical hydrogen bond the distances between oxygen of Ala18 and $C^{\gamma}H/C^{\delta}H_3$ groups of Leu22 increase (Figures 4d and 5e). In the LD simulations the order of the events sometimes differs from the order described; however, the necessary conditions for the α-helix → π-helix transition are (i) the g^+ rotameric state of Leu22 or Leu15 and (ii) the existence of the CO Met20−$H^{\gamma 1}$O Thr24 or the CO Leu13−$H^{\gamma 1}$O Thr17 hydrogen bond, respectively.

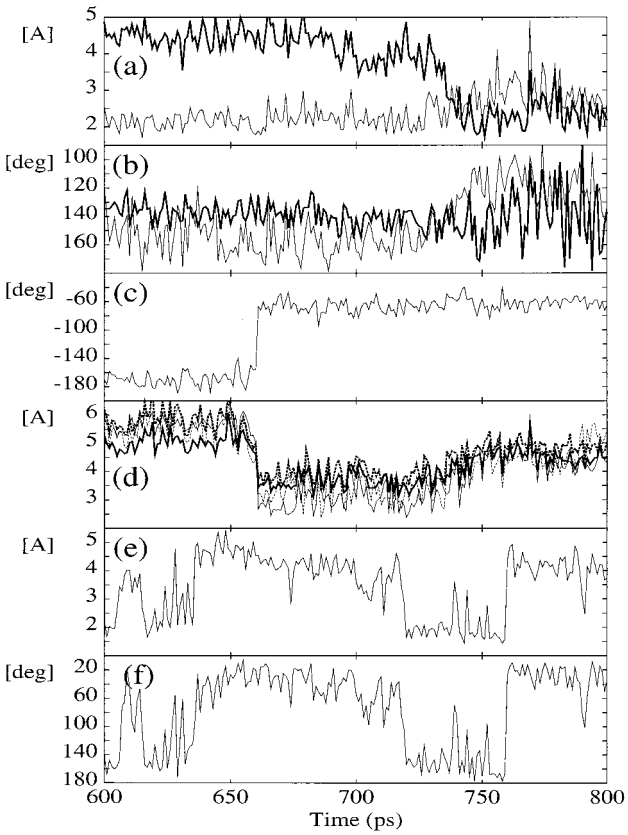

Figure 4. Selected parameters during the MD run, illustrating the formation of the first π-helical hydrogen bond (CO Ala18−NH Gly23): (a) HN Leu22−O Ala18 (thin line) and HN Gly23−O Ala18 (bold line) distances; (b) N Leu22−HN Leu22−O Ala18 (thin line) and N Gly23−HN Gly23−O Ala18 (bold line) hydrogen bond angles; (c) χ^1 angle of Leu22; (d) C^{γ} Leu22−O Ala18 (bold solid line), H^{γ} Leu22−O Ala18 (thin solid line), $C^{\delta 1}$ Leu22−O Ala18 (bold dashed line), and $H^{\delta 13}$ Leu22−O Ala18 (thin dashed line) distances; (e, f) hydrogen−acceptor distance and donor−hydrogen−acceptor angle in the backbone−side chain hydrogen bond between CO Met20 and $H^{\gamma 1}$O Thr24.

Although, the events occurring in the neighborhood of the glycine residues (21, 23, and 16) do not directly lead to the α-helix unfolding, these residues apparently play a major role in the α-helix unfolding. Indeed, Gly residues are known as a strong helix breakers because of the absence of the α-helix stabilizing interactions involving C^{β} and the largest loss of backbone conformational entropy during the α-helix formation (see Chakrabartty and Baldwin[45] and references therein). It is notable that in previous MD simulations of the first transmembrane helix of bacteriorhodopsin in vacuo, a number of flips of the backbone dihedral angles near the Gly residues were observed. Pervushin et al.[46] reported the distortion, observed during 90 ps of a 500 ps simulation, in which the angles ψ of Met20 and φ of Gly21 adopt positive values, inducing the kinked state of the helix. Iyer and Visheveshwara[47] observed similar flips of Gly21 and Gly23 φ and Leu22 ψ angles. In these distortions CO and NH groups, adjacent to the glycine

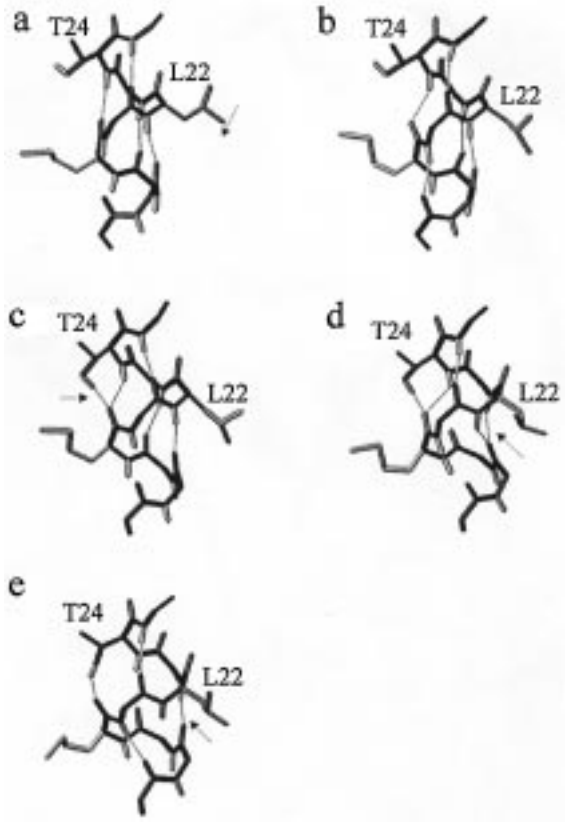

Figure 5. Selected snapshots of Thr17−Leu25 region of (1−36)-BR during the formation of the π-bulge: (a) 650 ps → (b) 662 ps, transition of Leu22 side chain from t to g^+ rotameric state; (c) 725 ps, CO Met20−$H^{\gamma 1}$O Thr24 hydrogen bond was formed; (d) 741 ps, bifurcated Ala18−Leu22 and Ala18−Gly23 hydrogen bonds are present; (e) 750 ps, first π-helical Ala18−Gly23 hydrogen bond was formed.

residues, do not participate in the system of α-helical hydrogen bonds. In our simulations several short (<5 ps), reversible flips of the backbone torsions to the positive values were observed near Gly residues (data not shown). However, these short-living distortions themselves do not induce unfolding of the α-helix and the formation of π-bulges.

The destabilizing effect of threonine residues seems to be mainly due to the formation of a hydrogen bond by the side chain in the g^+ ($\chi^1 \approx -60°$) rotameric state with the peptide backbone. Another source of the α-helix instability introduced by Thr as well as by other β-branched residues is the largest loss of the side chain conformational entropy during α-helix formation.[48,49] Namely, of three possible χ^1 rotamers allowed for these amino acids in the coil state, g^- and t for Ile and Thr and g^- and g^+ for Val are unfavorable in the α-helix because of the steric hindrance of their γ-atoms and the oxygen of the $i-3$ residue. It is notable that in LD simulations the populations of g^- and t rotamers of Thr17 and Thr24 increase with the increase of the dielectric permeability constant ϵ_o, apparently owing to the weakening of the side chain−backbone hydrogen bond.

Although the Leu residue is known to be one of the strongest helix formers, it also plays a role in the α-helix unfolding. For residues with a single C^γ atom only g^- rotamers are completely prohibited in α-helices.[49] Among t and g^+ rotamers g^+ is less favorable because of the small repulsive interaction between γ (and higher) groups and the oxygen of the preceding turn of the helix. Thus, flips between t and less favorable g^+ rotameric states of γ-branched Leu modulate the stability of the α-helix in Leu-Gly-Thr regions.

The analysis of the LD trajectories suggests that the short-range electrostatic interactions play a major role in the stabilization of the α-helix. The possibility of forming π-bulges seems to be determined by the balance between α-helix destabilizing factors and the strength of the α-helical hydrogen bonds. Indeed, g^+ rotamers of Leu22 and Leu15 together with the formation of side chain−backbone hydrogen bonds by Thr24 and Thr17 do not always lead to α-helix unfolding. In the most stable LD simulation ($\epsilon_o = 1$, $T = 300$ K) the population of side chain−backbone hydrogen bonds is 0.99 and populations of g^+ rotamers of Leu22 and Leu15 are 0.65 and 0.56, respectively; however, π-bulges are not formed. In the less stable LD trajectory ($\epsilon_o = 5$, $T = 300$ K) π-bulges also are not formed and the α-helix unfolds from the C-terminus. In the MD and LD ($\epsilon_o = 1$, $T = 500$ K and $\epsilon_o = 2-4$, $T = 300$ K) trajectories before the formation of π-helical hydrogen bonds, χ^1 of Leu22 (Leu15) exhibits several transitions. It is notable that the NMR structure analysis of (1−36)-BR in chloroform/methanol mixtures reveals CO Met20−$H^{\gamma 1}$O Thr24 and CO Leu13−$H^{\gamma 1}$O Thr17 hydrogen bonds and g^+ rotamers of Leu22 and Leu15.[29] This fact suggests the possibility of α-helix distortions due to the inherent instability of the corresponding regions of the α-helix in a weakly polar medium.

Time Scale of α-Helix Unfolding. NMR Order Parameters. In the "model-free" analysis of $^1H-^{15}N$ backbone NMR relaxation data at several magnetic fields, Orekhov et al.[31] observed substantial mobility of the α-helical part of (1−36)-BR (order parameters of ∼0.6) on the nanosecond time scale. The kinked states of the α-helix, formed in the above-described distortions, lead to substantial reorientations of the backbone $^1H-^{15}N$ vectors in the molecular coordinate frame. In all simulations (with the exception of LD with $\epsilon_o = 1$, $T = 300$ K and $\epsilon_o = 5$, $T = 300$ K) the distortions in the central part of the α-helix occur within several nanoseconds. This observation might suggest that the low order parameters of backbone $^1H-^{15}N$ vectors observed by Orekhov et al.[31] for (1−36)-BR in the chloroform/methanol mixture can be accounted for by the intermediate species arising on the way of the α-helix−random coil transition. However, a meaningful sampling of conformational space, required for correct modeling of $^1H-^{15}N$ NMR relaxation, is not possible at the current state. The limited number of events, observed both in MD and in LD simulations, cannot provide the numerical estimates of time scales of the transition.

Conclusions

The analysis of the MD and LD trajectories of the first transmembrane segment (1−36)-BR in a weakly polar medium shows that the unfolding of α-helix proceeds through the formation of local disturbed regions, stabilized by π-helical hydrogen bonds (π-bulges), in the central part of the peptide. The propagation of the π-bulges leads to metastable structures, intermediates of the α-helix−random coil transition. The mechanism of (1−36)-BR unfolding in chloroform/methanol mixtures is markedly different from those reported for water-soluble α-helical homopolymers and isolated α-helices of globular proteins. The specific unfolding of (1−36)-BR is determined by the amino acid composition of the transmembrane segment, which is rich in helix-breaking Gly and Thr residues. One can suggest that some of the intermediates of α-helix unfolding (such as small π-bulges), being stabilized by tertiary interactions in bacteriorhodopsin, might be of functional importance.

Acknowledgment. This work was supported by Russian Foundation for Basic Research, Grants 96-04-00054 and 96-04-50893 and ISSEP Grants a97-9699 and a98-2221.

Glossary

BR	bacteriorhodopsin
MD	molecular dynamics
LD	Langevin (stochastic) dynamics
NVT	constant number of atoms, volume, temperature
NPT	constant number of atoms, pressure, temperature
rmsd	root-mean-square deviation
RDF	radial distribution function
NMR	nuclear magnetic resonance

References and Notes

(1) Popot, J. L.; Engleman, D. M. *Biochemistry* **1990**, *29*, 4031.
(2) Popot, J. L.; Gerchman, S. E.; Engelman, D. M. *J. Mol. Biol*. **1987**, *198*, 655.
(3) Kahn, T. W.; Engleman, D. M. *Biochemistry* **1992**, *31*, 6144.
(4) Marti, T. *J. Biol. Chem*. **1998**, *273*, 9312.
(5) Pervushin, K. V.; Arseniev, A. S. *Bioorg. Khim. (Russia)* **1995**, *21*, 83.
(6) Tobias, D. J.; Brooks, C. L. *Biochemistry* **1991**, *30*, 6059.
(7) Young, W. S.; Brooks, C. L. *J. Mol. Biol*. **1996**, *259*, 560.
(8) Tirado-Rives, J.; Jorgensen, W. L. *Biochemistry* **1991**, *30*, 3864.
(9) Soman, K. V.; Karimi, A.; Case, D. A. *Biopolymers* **1991**, *31*, 1351.
(10) Dagget, V.; Levitt, M. *J. Mol. Biol*. **1992**, *233*, 1121.
(11) De Loof, H.; Nilsson, N.; Rigler, R. *J. Am. Chem. Soc*. **1992**, *114*, 4028.
(12) DiCapua, F. M.; Swaminathan, S.; Beveridge, D. L. *J. Am. Chem. Soc*. **1991**, *113*, 6145.
(13) Hirst, J. D.; Brooks, C. L. *Biochemistry* **1995**, *34*, 7614.
(14) Scholtz, J. M.; Baldwin, R. L. *Annu. Rev. Biophys. Biomol. Struct*. **1992**, *21*, 95.
(15) van Buuren, A. R.; Berendsen, H. J. C. *Biopolymers* **1993**, *33*, 1159.
(16) Kovacs, H.; Mark, A. E.; Johanson, J.; van Gunsteren, W. F. *J. Mol. Biol*. **1995**, *247*, 808.
(17) Shen, L.; Bassolino, D.; Stouch, T. *Biophys J*. **1997**, *73*, 3.
(18) Woolf, T. B. *Biophys. J*. **1997**, *73*, 2376.
(19) Belohorcova, K.; Davis, J. H.; Woolf, T. B.; Rouh, B. *Biophys. J*. **1997**, *73*, 3039.
(20) Tieleman, D. P.; Forrest, L. R.; Sansom, M. S.; Berendsen, H. J. C. *Biochemistry* **1998**, *37*, 17554.
(21) Tieleman, D. P.; Sansom, M. S.; Berendsen, H. J. C. *Biophys. J*. **1999**, *76*, 40.
(22) Duneau, J. P.; Grouzy, S.; Garnier, N.; Charpon, Y.; Genest, M. *Biophys. Chem.* **1999**, *76*, 35.
(23) Duneau, J. P.; Genest, D.; Genest, M. *J. Biomol. Struct. Dyn*. **1996**, *13*, 753.
(24) Deber, C. M.; Li, S. C. *Biopolymers* **1995**, *37*, 295.
(25) Liu, L. P.; Li, S. C.; Goto, N. K.; Deber, C. M. *Biopolymers* **1996**, *39*, 465.
(26) Li, S. C.; Deber, C. M. *FEBS Lett.* **1992**, *311*, 217.
(27) Li, S. C.; Goto, N. K.; Williams, K. A.; Deber, C. M. *Proc. Natl. Acad. Sci. U.S.A.* **1996**, *93*, 6676.
(28) Gratias, R.; Kessler, H. *J. Phys. Chem. B* **1998**, *102*, 2027.
(29) Pervushin, K. V.; Sobol, A. G.; Musina, L. Yu.; Abdulaeva, G. V.; Arseniev, A. S. *Mol. Biol. (Russia)* **1992**, *26*, 920.
(30) Orekhov, V. Yu.; Pervushin, K. V.; Korzhnev, D. M.; Arseniev, A. S. *J. Biomol. NMR* **1995**, *6*, 113.
(31) Orekhov, V. Yu.; Korzhnev, D. M.; Diercks, T.; Kessler, H.; Arseniev, A. S. *J. Biomol. NMR*, submitted.
(32) Dauber-Osguthorpe, P.; Roberts, V. A.; Osguthorpe, D. J.; Wolff, J.; Genest, M.; Hagler, A. T. *Proteins* **1988**, *4*, 31.
(33) Berendsen, H. J. C.; Postma, J. P. M.; van Gunsteren, W. F.; DiNola, A.; Haak, J. R. *J. Chem. Phys*. **1984**, *81*, 3684.
(34) Brooks, B. R.; Bruccoleri, R. E.; Olafson, B. D.; States, D. J.; Swamiathan, S.; Karplus, M. *J. Comput. Chem.* **1983**, *4*, 187.
(35) van Gunsteren, W. F.; Berendsen, H. J. C. *Mol. Phys*. **1977**, *34*, 1311.
(36) Brune, R. M.; van Gunsteren, W. F.; Bruschweiler, R.; Ernst, R. R. *J. Am. Chem. Soc*. **1993**, *115*, 4764.
(37) Schmidt, M. J.; Bruschweiler, R.; Ernst, R.; Dunbrack, R. L.; Joseph, D.; Karplus, M. *J. Am. Chem. Soc*. **1993**, *115*, 8747.
(38) Bremi, T.; Bruschweiler, R.; Ernst, R. R. *J. Am. Chem. Soc*. **1997**, *119*, 4272.
(39) Pervushin, K. V.; Orekhov, V. Yu.; Popov, A. I.; Musina, L. Yu.; Arseniev, A. S. *Eur. J. Biochem*. **1994**, *219*, 571.
(40) Keefe, L. J.; Sondek, J.; Shortle, D.; Lattman, E. E. *Proc. Natl. Acad. Sci. U.S.A.* **1993**, *90*, 3275.
(41) Eriksson, A. E.; Baase, W. A.; Zhang, X. J.; Heinz, D. W.; Blaber, M.; Baldwin, E. P.; Matthews, B. W. *Science* **1992**, *255*, 178.
(42) Yang, A. S.; Honig, B. *J. Mol. Biol*. **1995**, *252*, 351.
(43) Karasz, F. E.; Gajnos, G. E. *J. Phys. Chem*. **1973**, *77*, 1139.
(44) Bixon, M.; Lifson, S. *Biopolymers* **1966**, *4*, 815.
(45) Chakrabartty, A.; Baldwin, R. L. *Adv. Protein Chem*. **1995**, *46*, 141.
(46) Pervushin, K. V.; Orekhov, V. Yu.; Korzhnev, D. M.; Arseniev, A. S. *J. Biomol. NMR* **1995**, *5*, 383.
(47) Iyer, L. K.; Vishveshwara, S. *Biopolymers* **1996**, *38*, 401.
(48) Creamer, T. P.; Rose, G. D. *Proc. Natl. Acad. Sci. U.S.A.* **1992**, *89*, 5937.
(49) Pela, L.; Nemethy, G.; Sheraga, H. A. *Biopolymers* **1987**, *26*, 1273.